analytical chemistry

pubs.acs.org/ac

Article

Nanomolar Protein–Protein Interaction Monitoring with a Label-Free Protein-Probe Technique

Salla Valtonen,* Emmiliisa Vuorinen, Taru Kariniemi, Ville Eskonen, John Le Quesne, Martin Bushell, Harri Härmä, and Kari Kopra

Cite This: *Anal. Chem.* 2020, 92, 15781–15788

Read Online

ACCESS | Metrics & More | Article Recommendations | Supporting Information

ABSTRACT: Protein–protein interactions (PPIs) are an essential part of correct cellular functionality, making them increasingly interesting drug targets. While Förster resonance energy transfer-based methods have traditionally been widely used for PPI studies, label-free techniques have recently drawn significant attention. These methods are ideal for studying PPIs, most importantly as there is no need for labeling of either interaction partner, reducing potential interferences and overall costs. Already, several different label-free methods are available, such as differential scanning calorimetry and surface plasmon resonance, but these biophysical methods suffer from low to medium throughput, which reduces suitability for high-throughput screening (HTS) of PPI inhibitors. Differential scanning fluorimetry, utilizing external fluorescent probes, is an HTS compatible technique, but high protein concentration is needed for experiments. To improve the current concepts, we have developed a method based on time-resolved luminescence, enabling PPI monitoring even at low nanomolar protein concentrations. This method, called the protein probe technique, is based on a peptide conjugated with Eu^{3+} chelate, and it has already been applied to monitor protein structural changes and small molecule interactions at elevated temperatures. Here, the applicability of the protein probe technique was demonstrated by monitoring single-protein pairing and multiprotein complexes at room and elevated temperatures. The concept functionality was proven by using both artificial and multiple natural protein pairs, such as KRAS and eIF4A together with their binding partners, and C-reactive protein in a complex with its antibody.

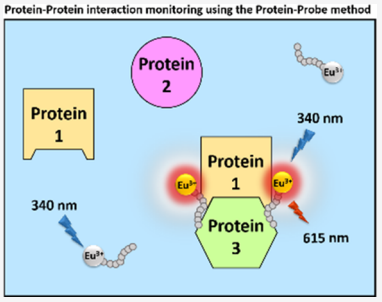

Protein–protein interactions (PPI) are essential to the normal function of a cell. The human genome can produce over one million different proteins utilizing, e.g., alternative splicing and machinery related to post-translational modifications.[1] The vast majority of these proteins function as a complex with one or more proteins. These complexes form an interaction network by, e.g., adjusting enzyme activity through signaling cascades, mediating physical motion through actin and myosin, and controlling the cell cycle.[2−4]

In addition to providing insights into cellular processes, the information on PPIs can also be applied for therapeutic purposes.[2,5] Historically, PPIs have been regarded as difficult drug targets, mostly because the interacting regions of PPIs are often flat and shallow, whereas small molecules often prefer binding to well-defined pockets, as in the case of enzymes and G-protein-coupled receptors, the most frequent drug targets today. This lack of clearly defined binding pockets makes PPIs difficult to target, especially for small molecule drugs. However, advanced methods are developed constantly to identify new ways to target PPIs. Such methodologies increase our understanding of PPI properties, enabling the development of novel types of drugs and mechanisms to control and study clinically relevant PPIs. Especially, high-throughput screening (HTS) methods are needed to effectively identify drug candidates for different PPIs.[6,7] As several methods are applied in parallel to validate screened hits, any newly developed methods can benefit the screening and validation process by filling demands related to simplicity, assay time, and cost-effectiveness.[8,9]

To this day, countless PPIs have been identified and studied with several types of PPI analysis methods. Traditionally, methods such as Förster resonance energy transfer (FRET), which rely on labeling the interacting components, have been extensively used to study PPIs also in a cellular context.[10,11] However, labeling the interacting components may interfere with the protein interactions. Thus, label-free methods have attracted increasing interest, as the interacting components are not labeled, providing increased flexibility for the detection of different PPI pairs and also new targets. These methods can be roughly divided as biophysical and luminescence-based methods.

Biophysical methods give information on, e.g., biomolecular structures and their dynamics and function, and the gold standard for PPIs and their interaction thermodynamics

Received: July 2, 2020
Accepted: November 17, 2020
Published: November 25, 2020

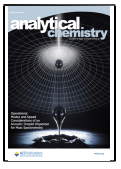

https://dx.doi.org/10.1021/acs.analchem.0c02823
Anal. Chem. 2020, 92, 15781–15788

monitoring is calorimetry. Both isothermal titration calorimetry and differential scanning calorimetry are often applied for PPIs,[12] but the disadvantage for these methods is the need for a relatively high micromolar protein concentration. Experiments are also delicate and is run in a carefully optimized and controlled environment. In addition, these methods are typically performed for individual samples, which is suboptimal for HTS.[12−16] Surface plasmon resonance (SPR) is another widely used technique originally developed for PPI studies. SPR has a relatively high sensitivity and is applicable to a large variety of different types of molecules within a wide concentration range. In SPR, one binding partner is immobilized onto the sensor surface, resembling a labeling procedure with similar potential problems. Even though SPR has higher throughput compared to the calorimetric methods, it is still not counted as a full HTS method. Regardless of the deficiencies, SPR is useful especially for fragment-based screening with a limited compound library size.[17,18]

Luminescence-based label-free methods utilize external probes and environmentally sensitive labels for detection. One of the main motivations for developing these methods has been the improved applicability for HTS compared to biophysical techniques. One such method is differential scanning fluorimetry (DSF), which relies on environmentally sensitive dyes to monitor the thermal stability of the studied protein in the presence and absence of interacting small molecular ligands (protein−ligand interaction, PLI) or proteins (PPI). SYPRO Orange is the most frequently used DSF dye today, as its spectral properties directly match the general laboratory hardware. SYPRO Orange luminescence is heavily quenched by water, but upon target protein denaturation, it binds to hydrophobic patches of the target protein. This binding-driven protection of SYPRO Orange increases the quantum yield, monitored as an increase in fluorescence.[19−21] Other dyes such as ANS (8-anilino-1-naphthalenesulfonic acid) and Nile Red have also been utilized in DSF measurements. These alternative dyes function highly similarly to SYPRO Orange, although, e.g., ANS has been reported to also interact with the cationic parts of the target protein.[21−24] Similar to differential scanning calorimetry, DSF monitors PPIs based on the thermal stability changes upon interaction. The main advantage of the DSF measurements over calorimetry is the HTS compatibility on a microtiter plate format.[19,20,25] The disadvantages are that not all PPIs provide a measurable thermal shift upon binding and that the DSF methods are material-consuming. The use of micromolar protein concentrations increases the risk of artifacts related to, e.g., spontaneous protein aggregation, simultaneously increasing the assay costs. Therefore, there has been an increasing need for more sensitive label-free probes with improved detection sensitivity and applicability to the HTS environment.

We have previously studied protein−protein interactions using time-resolved FRET (TR-FRET) and developed a quencher-modulated TR-FRET method enabling simultaneous monitoring of both PLI and PPI reactions.[26] In addition, we have recently introduced an external Eu^{3+}-labeled protein probe technique for the detection of protein stability and PLIs at a low nanomolar sensitivity level.[27] In this study, we introduce a further development of the protein probe for the detection of PPIs. The method is applicable not only for thermal but also for isothermal PPI detection, depending on the nature of the studied proteins or protein complexes. The label-free assay is HTS-compatible as performed in a microtiter plate format, and the simplicity of the method was highlighted using different disease relevant model PPI pairs, e.g., eukaryotic initiation factor 4A (eIF4A) and KRAS.

EXPERIMENTAL SECTION

The detailed list of materials and instrumentation, production and purification of proteins, Eu^{3+} conjugations, assay optimization, control assays, and data analysis are presented in the Supporting Information (SI). In addition, detailed protocols for model PPI reactions performed either at room temperature (RT) (streptavidin (SA)−biotinylated bovine serum albumin (BSA) and C-reactive protein (CRP)−monoclonal antibody (mAb)) or at elevated temperatures (CRP−mAb, KRAS−K27, and eukaryotic initiation factor 4A (eIF4A) either with eukaryotic translation initiation factor (eIF4H) or programmed cell death protein 4 (PDCD4)) are presented in the Supporting Information.

RESULTS AND DISCUSSION

Interactions between proteins are a fundamental part of correct cellular functionality, and impaired interactions may lead to various disease states. We have previously developed a label-free method for the detection of protein stability and PLIs,[27] which we now apply for PPI monitoring. The protein probe technique is based on a negatively charged Eu^{3+} chelate-labeled peptide (Eu^{3+} probe) used to measure protein structural changes, such as an increased surface area and exposed hydrophobic regions. Here, we introduce the protein probe technique in the context of PPIs (Figure 1), with the same Eu^{3+} probe in conditions optimized for PPI monitoring. The spectral studies of the Eu^{3+} probe and modulator showed the typical time-resolved luminescence (TRL) emission spectrum of the Eu^{3+} probe overlapping with the modulator excitation spectrum supplemented in the protein probe solution (Figure S1A). In the presence of two non-interacting proteins, the protein probe TRL signal is low, as the Eu^{3+} probe has a negligible interaction with intact individual proteins, leading to a considerably shortened luminescence lifetime (Figure S1B). However, upon protein pairing, the Eu^{3+} probe nanoenvironment changes, providing a contact surface for the Eu^{3+} probe binding. This results in an increased monitored TRL signal at room temperature (RT) or at elevated temperatures, depending on the size of the studied interaction complex.

Proof-of-Concept Streptavidin/Bio-BSA Assay Demonstrates the Protein Probe Technique for PPI Monitoring. PPIs are relatively difficult to monitor without excessive labeling and/or surface conjugation, and often they occur at a micromolar affinity level. To test the protein probe technique for PPI monitoring, we first selected model proteins with engineered interaction of unusually high binding affinity. Bio-BSA and SA, which form a large protein complex, were investigated as a proof-of-concept artificial protein pair. This ultrahigh affinity interaction enables, and also ensures, a maximal and basically irreversible binding, which is ideal for the assay demonstration.[28] To study this, 20 nM BSA or bio-BSA were assayed in an SA titration (10−600 nM). Under these conditions, no SA concentration-dependent TRL signal change was detected with non-interacting BSA (Figure 2A). However, a clear increase in the TRL signal was detected with bio-BSA when monitored under the same conditions at RT. The maximal signal was achieved at a 200 nM SA concentration, and no further signal change was observed at

https://dx.doi.org/10.1021/acs.analchem.0c02823
Anal. Chem. 2020, 92, 15781−15788

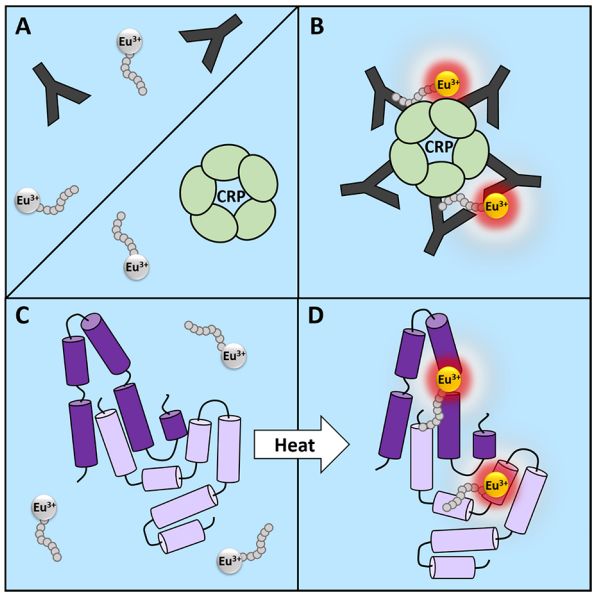

Figure 1. Protein-Probe technique for label-free protein−protein interaction monitoring. (A) Protein-Probe shows negligible binding to individual intact low-concentration proteins at room temperature (RT), monitored as a low TRL signal. (B) When the Protein-Probe is utilized for the detection of a large multiprotein complex, here, C-reactive protein (CRP) with its antibodies, the Eu^{3+} probe senses the increased surface area and a high TRL signal is observed at RT. (C) In the case of smaller proteins forming a 1:1 complex, a low TRL signal is monitored at RT, as the interaction cannot reshape the proteins sufficiently for Protein-Probe sensing. (D) However, upon heating, the protein−protein complex becomes more accessible for the Eu^{3+} probe binding, and the formation of a protein−protein pair is visible from the increase in the TRL signal and/or change in thermal stability.

higher SA concentrations. This indicates that the increased molecular weight and/or the nature of the formed complex had an impact on the binding properties of the Eu^{3+} probe and the detected TRL signal.

To prove the functionality, we next tested blocking the SA and bio-BSA interaction by performing biotin titration (0.01−10 μM). The assay was carried out with 200 nM SA and 20 nM bio-BSA, giving the maximal signal. We observed a biotin concentration-dependent reduction of the TRL signal with an S/B ratio of 34 calculated from the reactions with or without biotin (Figure 2B). This indicates the expected loss of bio-BSA interaction with SA in the presence of biotin. The observed IC_{50} value of 306 ± 4 nM is in accordance with the given SA concentration and demonstrates that the TRL signal response monitored was due to the artificial protein complexation, impaired by free biotin.

Antibody−Antigen Interaction at RT Is Detected Using the Protein Probe Technique. As the artificial model with SA and bio-BSA indicated protein probe functionality in PPI, we next studied a second high affinity PPI model: CRP interaction with anti-CRP mAb. CRP (0−100 nM) was first assayed with an anti-CRP mAb (0−500 nM) and also with two nonspecific mAbs as controls. The selected anti-CRP mAb has an ultrahigh picomolar level affinity for CRP binding.[29] Similar to the bio-BSA/SA pair, the binding between CRP and the specific anti-CRP mAb resulted in an increase in the TRL-signal at RT, whereas the nonspecific mAbs had no significant impact on the signal (Figure 3, Figure S2). Within the studied concentration ranges, the observed TRL signal between the protein complex and mAb alone peaked at the approximate ratio of 5:1 (mAb/CRP) independent of the protein concentration level. This is not surprising as CRP is known to have a pentameric structure. The maximal S/B ratio of 4.3, mAb/CRP complex vs mAb, was achieved with 20 nM CRP and 100 nM anti-CRP mAb, as at higher concentrations, the individual proteins already showed a minor increase in the signal without complexation (Figure S2). Also, this PPI model indicates that the relatively large protein complex provides a sufficient TRL signal change with the studied model systems when monitored at RT.

The Protein Probe Technique Measures Antibody−Antigen Interaction at Elevated Temperatures. Isothermal studies with the protein probe demonstrated that

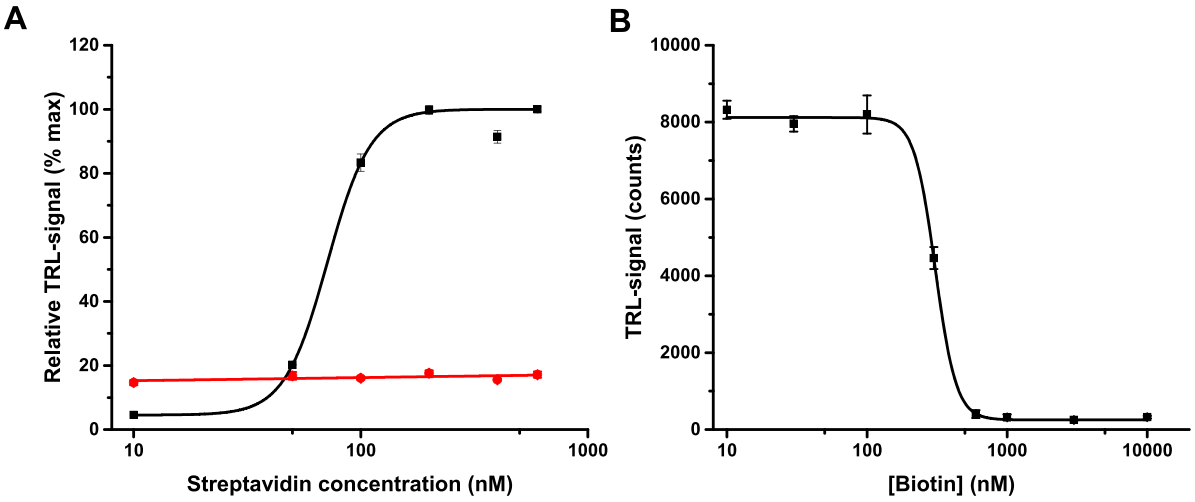

Figure 2. Bio-BSA interaction with streptavidin (SA) can be monitored using the Protein-Probe assay platform. (A) Assay performed with 20 nM BSA (red) or bio-BSA (black) and SA (10−600 nM) showed a clear increase in the TRL signal only in the case of bio-BSA, when monitored 5 min after the addition of the protein probe at RT. (B) Adding biotin (0.01−10 μM) reduced the TRL signal in the assay with 200 nM SA and 20 nM bio-BSA. This demonstrates the disintegration of the interaction between SA and bio-BSA when monitored at RT. Data from a single representative assay showing individual reactions (mean ± SD, n = 3).

https://dx.doi.org/10.1021/acs.analchem.0c02823
Anal. Chem. 2020, 92, 15781−15788

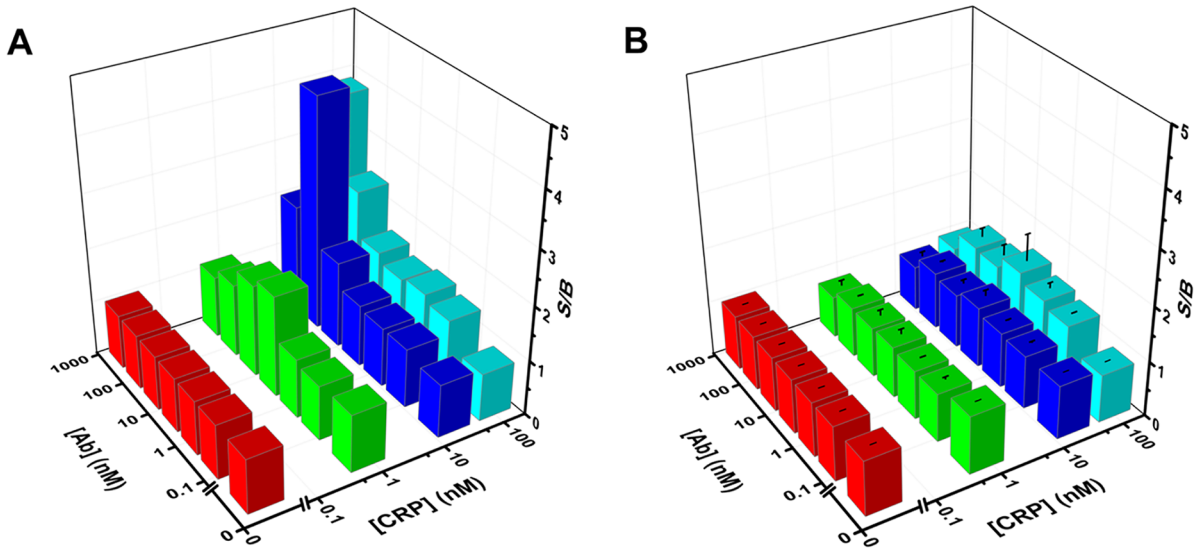

Figure 3. Protein probe technique can monitor CRP interaction with anti-CRP mAb at room temperature. (A) Interaction with CRP (0−100 nM) was monitored in titration with single anti-CRP mAb (0−500 nM) at RT. The optimal S/B ratio (mAb/CRP vs mAb) was obtained at a mAb/CRP ratio of 5:1, and the highest S/B ratio was obtained with 20 nM CRP and 100 nM mAb. (B) Nonspecific mAbs resulted in an insignificant signal change compared to CRP alone, as expected with no interaction. The TRL signals of the two nonspecific mAbs were highly similar (presented with error bars). Data are presented as an S/B ratio calculated from average signals (n = 3).

large complexes can be monitored at RT. Next, we tested the effect of elevated temperatures on the performance of the protein probe method by assaying CRP and mAb individually and in a complex for changes in the melting temperature (T_m). We have previously shown that an increase in the TRL signal is observed when a heated and denatured protein sample is monitored with the protein probe method, and we expected to measure an improved detectability with PPIs.[27] In all assays, the reactions are performed in biologically relevant buffers at RT, and thereafter the protein complex is heated to a given temperature. For the detection, the protein solution is reverted to RT by adding the protein probe solution.

We started the studies at elevated temperatures by determining the effect of mAb concentration to the signal and T_m (Figure S3). Although the mAb concentration had a drastic effect on the TRL signal level (Figure S3A), no major effect on T_m was observed at the measured concentration range (0.5−120 nM) (Figure S3B). Keeping in mind the signal level at RT and heating, we next tested the anti-CRP mAb (30 nM) and multiple CRP concentrations (0−150 nM) to observe the optimal protein ratio (Figure S4). The individually assayed two CRP concentrations (50 and 150 nM) and 30 nM mAb in complex with 150 nM CRP gave highly similar temperature profiles with T_m values of 56.0 ± 0.5, 58.8 ± 0.2, and 56.0 ± 1.0 °C, respectively. These values clearly follow the CRP melting without any significant information on the interaction. On the other hand, the lowest CRP concentration (5 nM) combined with mAb resulted in a similar T_m to mAb alone: 76.9 ± 1.0 and 77.8 ± 0.2 °C, respectively. No melting curve could be measured for 5 nM CRP. Interestingly, 50 nM CRP assayed with mAb gave a two-phase melting curve with T_m values of 58.1 ± 1.2 and 69.2 ± 0.4 °C. The first phase relates CRP melting, whereas the T_m of the second phase indicates CRP interaction with anti-CRP mAb (Figure S4A).

Unfortunately, the results obtained with mAb and various CRP concentrations provided no conclusive information on whether the binding has a measurable impact on the melting curve. Thus, we hypothesized that these concentrations might be too high to enable complex monitoring at elevated temperatures. To study this further, we selected two mAb concentrations (2 nM or 10 nM), which we assayed alone or with 1 and 5 nM or 5 and 10 nM CRP, respectively. At these concentrations, CRP was undetectable and mAb gave some measurable TRL signal (Figure S3). As hypothesized, a 4.2-fold TRL signal was measured when 2 nM mAb was assayed with 5 nM CRP and compared to the mAb alone at 90 °C (data not shown). This indicates that the interaction was detected, although the calculated T_m for mAb alone compared to in complex with CRP showed only a minor increase from 76.8 ± 0.1 to 79.1 ± 0.1 °C, respectively (data not shown). To study this further, we performed the assay using 10 nM anti-CRP mAb and nonspecific anti-hemoglobin mAb as the control. Both mAbs were assayed with 5 and 10 nM CRP (Figure S4B). At these concentrations, both mAbs were detectable, but the complex formation was monitored specifically with anti-CRP mAb and not with the nonspecific control. The signal increase with anti-CRP mAb was 7.4-fold with 5 nM CRP and 4.0-fold with 10 nM CRP, compared to nonspecific antihemoglobin mAb at 90 °C (Figure S4B). This indicates that the interaction was measurable at elevated temperatures for this stable, high-affinity antibody−antigen complex.

The Protein Probe Technique Monitors eIF4A Interaction at Elevated Temperatures. Following the CRP/mAb study, we chose to investigate more traditional PPI pairs with a significantly lower binding affinity. We selected eIF4A1 as the first target and monitored its interactions with two known binding partners, PDCD4 and eIF4H. eIF4A is a core translation initiation factor linking its ATPase activity to RNA helicase activity. It is a vital part of the eIF4F mRNA-cap-binding complex together with eIF4G and eIF4E, functioning as a main helicase in translation initiation.[30] eIF4A activity is modulated most notably by eIF4G, a scaffolding protein, and cofactor proteins eIF4H and eIF4B, which increase the helicase activity.[30,31] PDCD4, on the other hand, reduces eIF4A activity by blocking the RNA binding to the helicase and

https://dx.doi.org/10.1021/acs.analchem.0c02823
Anal. Chem. 2020, 92, 15781−15788

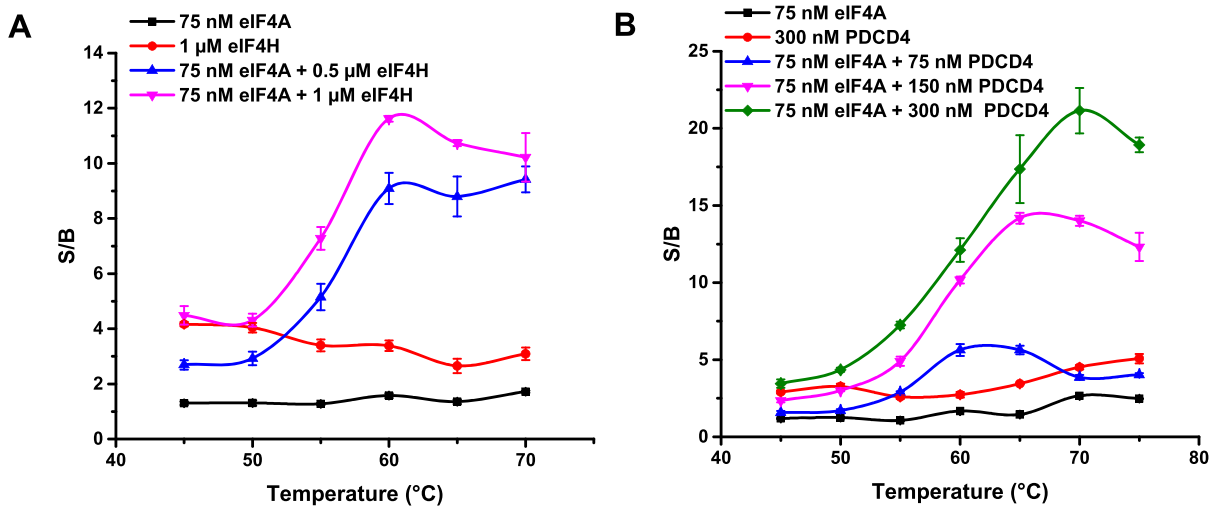

Figure 4. eIF4A interaction with eIF4H and PDCD4 could be detected using the protein probe technique. (A) Interaction between 75 nM eIF4A and 0.5 or 1 μM eIF4H was monitored in thermal ramping. eIF4A yielded no TRL signal and eIF4H yielded a low TRL signal when they were measured individually, but with an eIF4A/eIF4H complex, a high TRL signal was monitored at increased temperatures. (B) Interaction of 75 nM eIF4A and 75−300 nM PDCD4 was similarly observed as an increase in the TRL signal at elevated temperatures. At these concentrations, proteins did not produce thermal curves alone but only in complex. Data from a single representative assay showing individual reactions (mean ± SD, n = 3).

competing with eIF4G.[32,33] As eIF4H and PDCD4 differ in molecular weight, binding mode, and affinity to eIF4A,[34−37] we selected these two eIF4A-binding proteins to perform further studies with the protein probe technique.

Before conducting any binding assays, we determined the eIF4A functionality in a helicase assay with and without eIF4H and PDCD4 to ensure the protein quality and binding capacity. eIF4A was monitored with an equal amount of eIF4H using preannealed Cy3- and BHQ2-RNA and in the presence of excess DNA.[38,39] The eIF4H-induced increase in the eIF4A helicase activity was measured as an elevated FRET signal (Figure S5A). PDCD4 inhibitory activity was monitored in a similar assay using a 1:1 eIF4A:eIF4H complex in PDCD4 titration, and the monitored IC_{50} was 330 ± 8 nM for PDCD4 (Figure S5B). As all proteins showed expected functionality, we next determined the signal level and thermal stability properties of the individual proteins. Thermal melting assays were performed both with the protein probe and SYPRO Orange (Figure S6), and as previously,[27] the protein probe assays could be performed at lower concentrations compared to SYPRO Orange. The T_m values measured for eIF4A with the protein probe and SYPRO Orange were 54.5 ± 0.1 and 50.3 ± 0.1 °C, respectively.[40] In addition, we found that eIF4A detectability with the protein probe technique was improved by using Triton X-100 in the assay buffer. When the melting curve of 75 nM eIF4A was monitored using the protein probe without and with 0.001% Triton X-100, the S/B ratio at 65 °C was increased from 2.9 to 32.3, respectively. The corresponding T_m values were also monitored for PDCD4 and eIF4H. For PDCD4, T_m values were 59.7 ± 0.1 and 60.0 ± 0.3 °C with the protein probe and SYPRO Orange methods, respectively (data not shown). However, the results with eIF4H were nonconclusive with either method, and no clear thermal curve was detected (data not shown). To our knowledge, there are no reported T_m values for eIF4H and PDCD4.

As the affinity between eIF4A and the two selected interaction partners is in the submicromolar to micromolar level,[35−37] we selected 75 nM eIF4A1 to monitor interaction with eIF4H and PDCD4. Assays were performed in a buffer without Triton X-100, to reduce the assay sensitivity and to enable the use of higher protein concentrations. This selection was based on the mAb/CRP observation at high vs low concentrations (Figure S4). The thermal ramping with eIF4A was then performed using eIF4H and PDCD4 concentrations up to 1000 nM and 300 nM, respectively. Again, the interactions were carried out at RT before the complexes were heated. At the tested concentrations, eIF4H and PDCD4 gave only a modest signal when individual proteins were measured. However, when they were assayed in complex with eIF4A, a clear TRL signal increase was detected at elevated temperatures (Figure 4). Both protein complexes resulted in the highest S/B ratio at 65 °C when the complex was compared to individual eIF4H and PDCD4. S/B ratios of 5.5 and 4.0 were calculated for eIF4A interaction with 500 and 1000 nM eIF4H, respectively. PDCD4/eIF4A interaction was observed already at a 1:1 (75 nM) complex, but the interaction with higher (150 and 300 nM) PDCD4 concentrations resulted in increased S/B ratios of 10.5 and 5.0, respectively. In these assays, the monitored T_m value mostly followed the T_m of eIF4A alone, as the T_m values monitored with eIF4H and PDCD4 were 55.0 ± 0.2 and 56.4 ± 0.8 °C, respectively. Thus, ΔT of 0.5 and 1.9 °C were detected with eIF4H and PDCD4, respectively. As a control, 500 nM eIF4H and 150 nM PDCD4 were measured together at elevated temperatures (Figure S7). These proteins do not interact, and thus the S/B ratio of the complex did not significantly exceed that of the individual proteins when compared to the protein probe solution in buffer. This confirms that the measured PPI is specific in nature, and the TRL signal increase is not due to the revealed hydrophobic areas of the partially unfolded proteins or the increase in total protein concentration. The results also demonstrate that it is possible to monitor individual PPIs that have binding affinities in the common range for PPIs, even with relatively small proteins of different sizes (M_W ranging from 27.4 to 51.7 kDa) without forming large multiprotein complexes.

https://dx.doi.org/10.1021/acs.analchem.0c02823
Anal. Chem. 2020, 92, 15781−15788

KRAS Thermal Stabilization with DARPin K27 Is Observed with the Protein Probe Technique. Many interactions have been reported to produce a significant stabilizing effect in complex with a binding partner when compared to individual proteins, and the strategy has been successfully applied especially in PLI inhibitor screening.[41,42] We did not observe any major thermal shift with eIF4A and its binding partners, and thus we next chose to investigate KRAS, which is reported to be responsive to thermal stabilization.[43] As a KRAS interaction partner, we selected a guanosine diphosphate (GDP)-KRAS-specific designed ankyrin repeat protein (DARPin), K27, which is known to have inhibitory properties on KRAS activation and interactions with other proteins.[44] First, to prove the specificity and to estimate the binding affinity of K27 for KRAS, a quenching resonance energy transfer nucleotide exchange assay was performed using 50 nM KRAS.[26,45,46] Based on these results, IC_{50} values close to the KRAS concentration were calculated for K27 and also for GDP acting as a control (Figure S8). As only GDP showed a clear inhibitory curve with 5′-guanylyl imidodiphosphate (GMPPNP)-loaded KRAS, the results indicate that the affinity value for K27 is below 50 nM for GDP-KRAS and is significantly higher for GMPPNP-KRAS, which can thus be used as a control in interaction studies (Figure S8).[44]

As with eIF4A, KRAS was first studied using the protein probe side-by-side with SYPRO Orange to determine the appropriate concentration level for each individual method (Figure S9). Based on these experiments, we selected 50 nM KRAS for the protein probe interaction studies with K27. K27 yielded only low TRL signals at elevated temperatures due to its high thermal stability.[47] KRAS loaded with GDP or GMPPNP were next measured with the protein probe or SYPRO Orange in thermal denaturation. The calculated T_m values of 50 nM KRAS with the protein probe were 62.7 ± 0.3 and 53.0 ± 0.4 °C for GDP- and GMPPNP-KRAS, respectively (Figure 5). These T_m values were further confirmed with SYPRO Orange using 3 μM KRAS, giving T_m values of 58.6 ± 0.4 and 50.1 ± 0.6 °C for GDP- and GMPPNP-KRAS, respectively (data not shown). As K27 affinity was at a low nanomolar level (Figure S8), we selected 100 nM K27 for interaction assays with KRAS. This concentration is expected to provide near complete saturation and thus enables high response when interacting with KRAS. In a thermal assay with the protein probe, a K27-dependent T_m shift in the KRAS denaturation curve was monitored with GDP-KRAS but not with the GMPPNP-KRAS used as a control (Figure 5). ΔT monitored with GDP-KRAS was 8.7 °C, whereas with GMPPNP-KRAS it was negligible (0.3 °C). This thermal shift demonstrates K27-specific interaction with GDP-KRAS, and that the KRAS is thermally stabilized upon interaction. These results were further confirmed using SYPRO Orange (data not shown), and together, these results demonstrate the potential of the protein probe technique to monitor different types of PPIs.

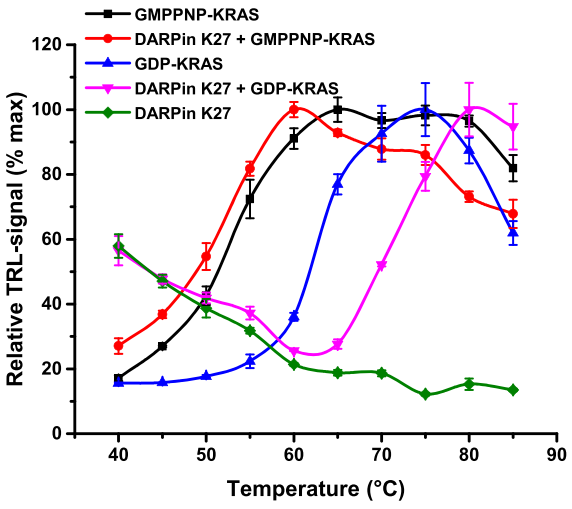

Figure 5. KRAS stability increase upon K27 DARPin interaction monitored with the protein probe assay. KRAS (50 nM) loaded with GMPPNP and GDP were monitored individually or in the complex with 100 nM K27, a GDP-KRAS-specific DARPin. The GMPPNP-KRAS T_m was not affected by K27, whereas the stability of GDP-KRAS was increased significantly, ΔT = 8.7 °C. K27 did not produce a signal at the elevated temperature. Data from a single representative assay showing individual reactions (mean ± SD, n = 3).

Here, we presented the protein probe technique for the monitoring of PPIs possessing binding affinities from the picomolar to micromolar level. The method can be applied for the detection of dimeric and multimeric interactions at room and elevated temperatures. All interactions were performed at RT, but with smaller protein pairs of a relatively small size, the complex formation can be detected by taking advantage of the increasing temperature. Using the eIF4A translation initiation factor, we demonstrated that PPIs occurring without significant thermal stabilization can also be monitored. On the other hand, the ability to monitor KRAS thermal stabilization was demonstrated in the presence of K27 DARPin. With both natural and artificial model systems, we were able to demonstrate PPI monitoring using multiple different concepts by varying the temperature and adjusting the protein concentration to an appropriate level to support each detection method. Further studies are needed to prove the assay functionality as an HTS tool for PPI inhibitor screening and for alternative type PPI formats. However, the functionality in the microtiter plate format provides a good starting point for these assays and for further studies to understand the mechanism behind the method to improve its function.

CONCLUSIONS

We have demonstrated the applicability of the protein probe for PPI monitoring using nanomolar protein concentrations and various protein pairs with different binding properties. The external Eu^{3+} probe differentiates individual and interacting proteins by providing high TRL signals after protein−protein complexation. The protein probe was demonstrated to detect PPIs at room and elevated temperatures depending on the protein complex. The method was shown to have high sensitivity compared to reference methods, enabling lowered protein consumption and thus leading to less expensive assays with a lower risk of aggregation-mediated artifacts. The method can potentially be used for general protein interaction studies and, after careful studies to prove the method robustness, also for PPI inhibitor screening in an HTS format. In the future, the protein probe method is also expected to provide an efficient tool for monitoring other types of interactions, e.g., protein aggregation.

https://dx.doi.org/10.1021/acs.analchem.0c02823
Anal. Chem. 2020, 92, 15781−15788

■ ASSOCIATED CONTENT

Supporting Information

The Supporting Information is available free of charge at https://pubs.acs.org/doi/10.1021/acs.analchem.0c02823.

Additional materials and methods and supporting graphs (PDF)

■ AUTHOR INFORMATION

Corresponding Author

Salla Valtonen − *Department of Chemistry, Chemistry of Drug Development, University of Turku, 20500 Turku, Finland;* orcid.org/0000-0002-4948-7169; Email: samaval@utu.fi

Authors

Emmiliisa Vuorinen − *Department of Chemistry, Chemistry of Drug Development, University of Turku, 20500 Turku, Finland*

Taru Kariniemi − *Department of Chemistry, Chemistry of Drug Development, University of Turku, 20500 Turku, Finland*

Ville Eskonen − *Department of Chemistry, Chemistry of Drug Development, University of Turku, 20500 Turku, Finland;* orcid.org/0000-0001-5214-5904

John Le Quesne − *University of Cambridge, Leicester LE1 7HB, U.K.*

Martin Bushell − *Cancer Research U.K. Beatson Institute, Glasgow G61 1BD, U.K.; Institute of Cancer Sciences, University of Glasgow, Glasgow G61 1QH, U.K.*

Harri Härmä − *Department of Chemistry, Chemistry of Drug Development, University of Turku, 20500 Turku, Finland;* orcid.org/0000-0002-8936-039X

Kari Kopra − *Department of Chemistry, Chemistry of Drug Development, University of Turku, 20500 Turku, Finland;* orcid.org/0000-0001-7585-6020

Complete contact information is available at: https://pubs.acs.org/10.1021/acs.analchem.0c02823

Notes

The authors declare the following competing financial interest(s): K.K. and H.H. have commercial interest through QRET Technologies.

■ ACKNOWLEDGMENTS

This work was supported by the Academy of Finland (296225, 329012, 323433, and 296093), Medical Research Council Technology (LifeArc)−Development Gap Fund, Instrumentarium Science Foundation, Drug Research Doctoral Programme of the University of Turku, Finnish Concordia Fund, Finnish Academy of Science and Letters (foundation of Vilho, Yrjö, and Kalle Väisälä), and Cancer Research U.K. (A17196 and A29252). We thank Dr. William Gillette from Leidos Biomedical Research, Inc. and Frederick National Laboratory for Cancer Research for providing us KRAS and the related proteins.

■ ABBREVIATIONS

BSA	bovine serum albumin
CRP	C-reactive protein
DARPin	designed ankyrin repeat protein
DSF	differential scanning fluorimetry
eIF4A	eukaryotic initiation factor 4A
eIF4H	eukaryotic translation initiation factor 4H
FRET	Förster resonance energy transfer
GDP	guanosine diphosphate
GMPPNP	5′-guanylyl imidodiphosphate
HTS	high-throughput screening
mAb	monoclonal antibody
PDCD4	programmed cell death protein 4
PLI	protein−ligand interaction
PPI	protein−protein interaction
RT	room temperature
SA	streptavidin
SPR	surface plasmon resonance
TRL	time-resolved luminescence
TR-FRET	time-resolved Förster resonance energy transfer

■ REFERENCES

(1) Jensen, O. N. *Curr. Opin. Chem. Biol.* **2004**, *8*, 33−41.
(2) Braun, P.; Gingras, A.-C. *Proteomics* **2012**, *12*, 1478−1498.
(3) Berggård, T.; Linse, S.; James, P. *Proteomics* **2007**, *7*, 2833−2842.
(4) Piazza, I.; Kochanowski, K.; Cappelletti, V.; Fuhrer, T.; Noor, E.; Sauer, U.; Picotti, P. *Cell* **2018**, *172*, 358−372.e23.
(5) Wells, J. A.; McClendon, C. L. *Nature* **2007**, *450*, 1001−1009.
(6) Ran, X.; Gestwicki, J. E. *Curr. Opin. Chem. Biol.* **2018**, *44*, 75−86.
(7) Bojadzic, D.; Buchwald, P. *Curr. Top. Med. Chem.* **2018**, *18*, 674−699.
(8) Turnbull, A. P.; Boyd, S. M.; Walse, B. *Res. Rep. Biochem.* **2014**, *4*, 13.
(9) Scott, D. E.; Ehebauer, M. T.; Pukala, T.; Marsh, M.; Blundell, T. L.; Venkitaraman, A. R.; Abell, C.; Hyvönen, M. *ChemBioChem* **2013**, *14*, 332−342.
(10) Lin, W.; Chen, T. *Adv. Protein Chem. Struct. Biol.* **2018**, *110*, 31−63.
(11) Okamoto, K.; Sako, Y. *Curr. Opin. Struct. Biol.* **2017**, *46*, 16−23.
(12) Cooper, M. A. *Anal. Bioanal. Chem.* **2003**, *377*, 834−842.
(13) Jelesarov, I.; Bosshard, H. R. *J. Mol. Recognit.* **1999**, *12*, 3−18.
(14) Johnson, C. M. *Arch. Biochem. Biophys.* **2013**, *531*, 100−109.
(15) Chiu, M. H.; Prenner, E. J. *J. Pharm. BioAllied. Sci.* **2011**, *3*, 39−59.
(16) Durowoju, I. B.; Bhandal, K. S.; Hu, J.; Carpick, B.; Kirkitadze, M. *J. Visualized Exp.* **2017**, *121*, 55262.
(17) Drescher, D. G.; Selvakumar, D.; Drescher, M. J. *Adv. Protein Chem. Struct. Biol.* **2018**, *110*, 1−30.
(18) Willander, M.; Al-Hilli, S. *Methods Mol. Biol.* **2009**, *544*, 201−229.
(19) Niesen, F. H.; Berglund, H.; Vedadi, M. *Nat. Protoc.* **2007**, *2*, 2212−2221.
(20) Huynh, K.; Partch, C. L. *Curr. Protoc. Protein Sci.* **2015**, *79*, 28.
(21) Lang, B. E.; Cole, K. D. *Biotechnol. Prog.* **2017**, *33*, 677−686.
(22) Hawe, A.; Sutter, M.; Jiskoot, W. *Pharm. Res.* **2008**, *25*, 1487−1499.
(23) Sackett, D. L.; Wolff, J. *Anal. Biochem.* **1987**, *167*, 228−234.
(24) Gasymov, O. K.; Glasgow, B. J. *Biochim. Biophys. Acta, Proteins Proteomics* **2007**, *1774*, 403−411.
(25) Lavinder, J. J.; Hari, S. B.; Sullivan, B. J.; Magliery, T. J. *J. Am. Chem. Soc.* **2009**, *131*, 3794−3795.
(26) Kopra, K.; Vuorinen, E.; Abreu-Blanco, M.; Wang, Q.; Eskonen, V.; Gillette, W.; Pulliainen, A. T.; Holderfield, M.; Härmä, H. *Anal. Chem.* **2020**, *92*, 4971−4979.
(27) Vuorinen, E.; Valtonen, S.; Eskonen, V.; Kariniemi, T.; Jakovleva, J.; Kopra, K.; Härmä, H. *Anal. Chem.* **2020**, *92*, 3512−3516.
(28) Weber, P. C.; Ohlendorf, D. H.; Wendoloski, J. J.; Salemme, F. R. *Science* **1989**, *243*, 85−88.
(29) Kåpyaho, K.; Tanner, P.; Kårkkåinen, T.; Weber, T. *Scand. J. Clin. Lab. Invest.* **2009**, *49*, 389−393.
(30) Hinnebusch, A. G.; Lorsch, J. R. *Cold Spring Harbor Perspect. Biol.* **2012**, *4*, a011544.

(31) Jackson, R. J.; Hellen, C. U. T.; Pestova, T. V. *Nat. Rev. Mol. Cell. Biol.* **2010**, *11*, 113−127.
(32) Yang, H.-S.; Jansen, A. P.; Komar, A. A.; Zheng, X.; Merrick, W. C.; Costes, S.; Lockett, S. J.; Sonenberg, N.; Colburn, N. H. *Mol. Cell. Biol.* **2003**, *23*, 26−37.
(33) Lankat-Buttgereit, B.; Göke, R. *Biol. Cell* **2009**, *101*, 309−317.
(34) Rogers, G. W., Jr.; Richter, N. J.; Lima, W. F.; Merrick, W. C. *J. Biol. Chem.* **2001**, *276*, 30914−30922.
(35) Loh, P. G.; Yang, H.-S.; Walsh, M. A.; Wang, Q.; Wang, X.; Cheng, Z.; Liu, D.; Song, H. *EMBO J.* **2009**, *28*, 274−285.
(36) Waters, L. C.; Strong, S. L.; Ferlemann, E.; Oka, O.; Muskett, F. W.; Veverka, V.; Banerjee, S.; Schmedt, T.; Henry, A. J.; Klempnauer, K.-H.; Carr, M. D. *J. Biol. Chem.* **2011**, *286*, 17270−17280.
(37) Marintchev, A.; Edmonds, K. A.; Marintcheva, B.; Hendrickson, E.; Oberer, M.; Suzuki, C.; Herdy, B.; Sonenberg, N.; Wagner, G. *Cell* **2009**, *136*, 447−460.
(38) Özeş, A. R.; Feoktistova, K.; Avanzino, B. C.; Fraser, C. S. *J. Mol. Biol.* **2011**, *412*, 674−687.
(39) Wilczynska, A.; Gillen, S. L.; Schmidt, T.; Meijer, H. A.; Jukes-Jones, R.; Langlais, C.; Kopra, K.; Lu, W.-T.; Godfrey, J. D.; Hawley, B. R.; Hodge, K.; Zanivan, S.; Cain, K.; Le Quesne, J.; Bushell, M. *Genome Biol.* **2019**, *20*, 262.
(40) Chu, J.; Galicia-Vázquez, G.; Cencic, R.; Mills, J. R.; Katigbak, A.; Porco, J. A., Jr.; Pelletier, J. *Cell Rep.* **2016**, *15*, 2340−2347.
(41) Lo, M.-C.; Aulabaugh, A.; Jin, G.; Cowling, R.; Bard, J.; Malamas, M.; Ellestad, G. *Anal. Biochem.* **2004**, *332*, 153−159.
(42) Pantoliano, M. W.; Petrella, E. C.; Kwasnoski, J. D.; Lobanov, V. S.; Myslik, J.; Graf, E.; Carver, T.; Asel, E.; Springer, B. A.; Lane, P.; Salemme, F. R. *J. Biomol. Screening* **2001**, *6*, 429−440.
(43) Zeng, M.; Lu, J.; Li, L.; Feru, F.; Quan, C.; Gero, T. W.; Ficarro, S. B.; Xiong, Y.; Ambrogio, C.; Paranal, R. M.; Catalano, M.; Shao, J.; Wong, K.-K.; Marto, J. A.; Fischer, E. S.; Jänne, P. A.; Scott, D. A.; Westover, K. D.; Gray, N. S. *Cell Chem. Biol.* **2017**, *24*, 1005−1016.e3.
(44) Guillard, S.; Kolasinska-Zwierz, P.; Debreczeni, J.; Breed, J.; Zhang, J.; Bery, N.; Marwood, R.; Tart, J.; Overman, R.; Stocki, P.; Mistry, B.; Phillips, C.; Rabbitts, T.; Jackson, R.; Minter, R. *Nat. Commun.* **2017**, *8*, 16111.
(45) Kopra, K.; Ligabue, A.; Wang, Q.; Syrjänpää, M.; Blaževitš, O.; Veltel, S.; Van Adrichem, A. J.; Hänninen, P.; Abankwa, D.; Härmä, H. *Anal. Bioanal. Chem.* **2014**, *406*, 4147−4156.
(46) Kopra, K.; Van Adrichem, A. J.; Salo-Ahen, O. M. H.; Peltonen, J.; Wennerberg, K.; Härmä, H. *Anal. Chem.* **2017**, *89*, 4508−4516.
(47) Binz, H. K.; Amstutz, P.; Kohl, A.; Stumpp, M. T.; Briand, C.; Forrer, P.; Grütter, M. G.; Plückthun, A. *Nat. Biotechnol.* **2004**, *22*, 575−582.

https://dx.doi.org/10.1021/acs.analchem.0c02823
Anal. Chem. 2020, 92, 15781−15788